minerals

MDPI

Article

Berthierine-2H_1 from Lovozero Alkaline Massif, Kola Peninsula, Russia: First Structure Model for Berthierine and Complexity-Stability Relations

Sergey V. Krivovichev [1,2,*], Victor N. Yakovenchuk [1,3], Olga F. Goychuk [1,3], Yakov A. Pakhomovskii [1,3] and Vladimir G. Krivovichev [4]

[1] Nanomaterials Research Center, Kola Science Center, Russian Academy of Sciences, Fersmana Str. 14, Apatity 184209, Russia; v.yakovenchuk@ksc.ru (V.N.Y.); o.goychuk@ksc.ru (O.F.G.); y.pakhomovskiy@ksc.ru (Y.A.P.)
[2] Department of Crystallography, Institute of Earth Sciences, St. Petersburg State University, University Emb. 7/9, St. Petersburg 199034, Russia
[3] Geological Institute, Kola Science Center, Russian Academy of Sciences, Fersmana Str. 14, Apatity 184209, Russia
[4] Department of Mineralogy, Institute of Earth Sciences, St. Petersburg State University, University Emb. 7/9, St. Petersburg 199034, Russia; vkrivovi@yandex.ru
* Correspondence: skrivovi@mail.ru

Abstract: Berthierine was found in a natrolite vein intersecting volcanogenic-sedimentary rocks on the slope of Mt. Quamdespakh in the upper reaches of the Suolwai River, Lovozero alkaline massif, Kola peninsula, Russian Arctic. The mineral occurs as well-formed translucent pyramidal crystals up to 250 μm in size. The chemical composition determined by electron microprobe analysis corresponds to the empirical formula $^{VI}(Fe^{2+}_{1.99}Al_{0.94}Mg_{0.03}Mn_{0.04})_{\Sigma 3.00}[^{IV}(Si_{1.15}Al_{0.85})_{\Sigma 2.00}O_5]$ $[(OH)_{3.92}O_{0.08}]_{\Sigma 4.00}$; the idealized formula is $^{VI}(Fe^{2+}{}_2Al)[^{IV}(SiAl)O_5](OH)_4$. The crystal-structure determination (the first detailed crystal-structure characterization of berthierine) shows that the Lovozero mineral is hexagonal, $P6_3cm$ (a = 5.3903(4), c = 14.0146(10) Å, V = 352.64(6) Å^3, R_1 = 0.053 for 338 unique observed reflections), and corresponds to the 2H_1 polytype of serpentine-group minerals with 1:1 tetrahedral-octahedral layers. The unit cell contains two $M_3[T_2O_5](OH)_4$ layers (M = Fe^{2+},Al; T = Si,Al) stacked along the c axis. The calculations of information-based structural and topological complexity parameters indicate that berthierine is structurally and topologically simpler than its chlorite-group polymorph chamosite. Since berthierine usually crystallizes metastably in the stability field of chamosite, the complexity analysis is agreement with the Goldsmith rule that states that, in Ostwald sequences of crystallization, metastable phases are simpler and more disordered than their stable counterparts. This observation can be applied to a general case of the metastable formation of serpentine-group minerals prior to the crystallization of chlorites.

Keywords: berthierine; crystal structure; Kola peninsula; Arctic; chamosite; metastability; structural complexity; Goldsmith principle

Academic Editor: Manuel Munoz

Received: 5 December 2024
Revised: 22 December 2024
Accepted: 25 December 2024
Published: 26 December 2024

Citation: Krivovichev, S.V.; Yakovenchuk, V.N.; Goychuk, O.F.; Pakhomovskii, Y.A.; Krivovichev, V.G. Berthierine-2H_1 from Lovozero Alkaline Massif, Kola Peninsula, Russia: First Structure Model for Berthierine and Complexity-Stability Relations. *Minerals* **2025**, *15*, 13. https://doi.org/10.3390/min15010013

1. Introduction

Berthierine, or $(Fe^{2+},Fe^{3+},Al)_3(Si,Al)_2O_5(OH)_4$, is a 1:1 layered silicate that belongs to the serpentine subgroup of the kaoline-serpentine group. It has been found in a number of different geological environments, mostly in low-temperature sedimentary formations, including laterites [1,2], polar soils [3], coal measures [4], bauxites (where it may occur as

a rock-forming mineral) [5–8], siderite sediments [9], etc. Berthierine is also known as a secondary mineral formed as a result of alteration of primary Fe-Mg silicate minerals [10–13]. The hydrothermal origin of berthierine was reported for pegmatites [14,15].

In low-temperature environments, berthierine forms metastably as a precursor to chamosite, its polymorph that belongs to the chlorite group. The studies of the thermodynamic properties of berthierine and chamosite [16–20] indeed demonstrate that the latter is stable in relation to the former. It has also been observed experimentally that a serpentine-group mineral usually forms metastably prior to the formation of a chlorite-group mineral [16,18,21,22], obeying the famous Ostwald rule of stages [23–27]. J. Goldsmith [28] proposed that metastable polymorphs forming in the Ostwald cascade of phases are usually structurally simpler than their stable counterparts, which was confirmed through the recent application of information-based structural complexity measures [29–38]. It is of interest to verify whether the Goldsmith principle holds for the pair of berthierine (metastable) and chamosite (stable). However, despite the mineralogical and petrological importance of berthierine, information about its crystallography and crystal chemistry is very scarce [16,39] with no full crystal-structure determination of the mineral reported so far. The obvious reason for this lacune in data is the mode of occurrence of berthierine, which is usually found as fine-grained aggregates intermixed or intergrown with other minerals. Herein, we report on the find of berthierine in pegmatites of the Lovozero alkaline massif, Kola peninsula, Russia, where the mineral occurs in crystals of good enough quality to be studied using modern X-ray diffraction crystallography equipment. We provide a full mineralogical, chemical, and structural description of the sample and discuss the validity of the Goldsmith principle for the metastable formation of berthierine.

2. Materials and Methods

2.1. Materials

The crystals of berthierine studied in this work originated from the Lovozero alkaline massif, Kola peninsula, Russian Arctic [15]. The mineral was found in a natrolite vein intersecting volcanogenic-sedimentary rocks on the slope of Mt. Quamdespahk in the upper reaches of the Suolwai River. Bertierine is represented by well-formed translucent pyramidal crystals up to 250 μm in size (Figure 1a,b), fine-grained mass of xenomorphic excretions up to 0.4 mm, as well as paramorphoses in magnetite crystals among natrolite crystals. The replacement of berthierine by clay minerals is observed. The association includes loparite-(Ce), minerals of the ilmenite-pyrophanite series, zircon, fluorapatite, pyrrhotite, and rhabdophane-(Ce). Along with this, small (up to 100 μm) nests are observed, composed of the smallest (less than 1 μm) crystals of berthierine and baddeleyite. Berthierine forms pyramidal crystals with the $\{20\bar{2}1\}$, $\{000\bar{1}\}$, and {0001} forms (Figure 1c–f). Intergrowth or twins on {0001} are common (Figure 1c,f).

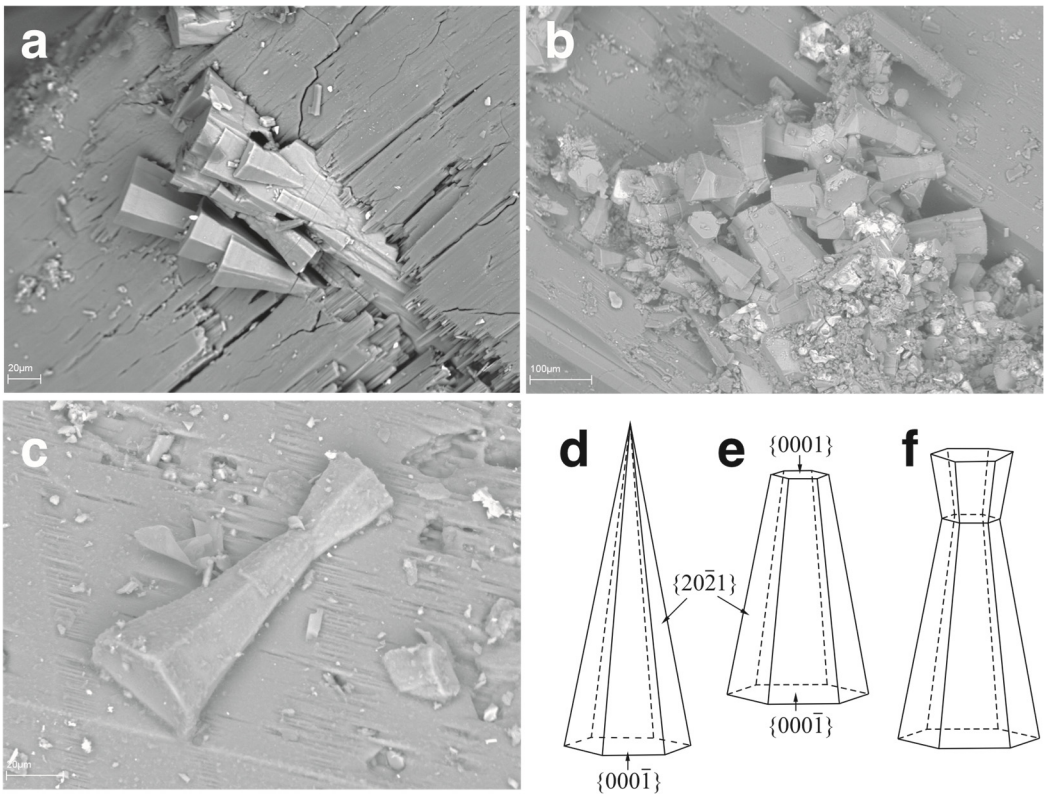

Figure 1. Crystal morphologies and occurrence of berthiertine from Lovozero massif, Kola peninsula, Russia: crystals of berthierine on the surface of natrolite (**a**,**b**); oriented intergrowth (or twin) of two crystals of berthierine along the (0001) face (**c**); hexagonal pyramidal crystals with and with no (0001) face ((**d**) and (**e**), respectively); scheme showing orientation of two crystals intergrown along the (0001) face (**f**).

2.2. Chemical Composition

Several crystals of berthierine were mounted in epoxy blocks and polished. The elemental analysis was carried out using scanning electron microscope LEO-1450 (Carl Zeiss Microscopy, Jena, Germany) equipped with an energy-dispersive spectrometer ULTIM MAX 100 (OXFORD Instruments, Great Britain, Abingdon, UK) at an accelerating voltage of 20 kV, with a probe current of 2 nA. The results are given in Table 1. The energy-dispersive spectra were processed automatically using the AzTec Energy software package. The following standards were used: pyrope (Mg, Al), wollastonite (Si), hematite (Fe), and synthetic $MnCO_3$ (Mn).

The average empirical chemical formula calculated on the basis of Fe + Mn + Mg + Al + Si = 5 can be written as $^{VI}(Fe^{2+}_{1.99}Al_{0.94}Mg_{0.03}Mn_{0.04})_{\Sigma 3.00}[^{IV}(Si_{1.15}Al_{0.85})_{\Sigma 2.00}O_5][(OH)_{3.92}O_{0.08}]_{\Sigma 4.00}$; the idealized formula is $^{VI}(Fe^{2+}{}_2Al)[^{IV}(SiAl)O_5](OH)_4$, where VI and IV indicate octahedral and tetrahedral sites, respectively. Both empirical and chemical formulas are in agreement with the results of crystal-structure determination (see below). Brindley [40] recommended calculation of the chemical formulae of berthierine on the basis of the total valence of cations in octahedral and tetrahedral positions equal to 14+, assuming possibility of vacancies in the cation sites. No vacancies have been observed in the Lovozero berthierine on the basis of crystal-structure analysis, so the formula was calculated based on the 5 cation sites.

Table 1. Chemical composition (in wt.%) of berthierine from Lovozero.

	1	2	3
SiO_2	19.59	19.95	20.01
Al_2O_3	26.16	26.08	26.97
FeO *	40.79	41.84	40.54
MgO	0.41	0.34	0.34
MnO	0.87	0.89	1.00
H_2O **	10.29	10.42	10.43
Total	98.89	99.52	99.29
Si	1.14	1.15	1.15
^{IV}Al	0.86	0.85	0.85
Total	2.00	2.00	2.00
^{VI}Al	0.93	0.92	0.98
Fe	1.99	2.01	1.95
Mg	0.04	0.03	0.03
Mn	0.04	0.04	0.05
Total	3.00	3.00	3.00
OH	3.92	3.97	3.94
O	5.08	5.03	5.06
Total	9.00	9.00	9.00

* Total Fe as FeO; ** calculated from stoichiometry.

2.3. Single-Crystal X-Ray Diffraction Analysis

The crystal-structure study of berthierine was carried out by means of the Synergy S single-crystal diffractometer equipped with the Hypix detector using monochromatic Mo$K\alpha$ radiation (λ = 0.71069 Å) at room temperature. More than half of the diffraction sphere was collected with scanning step of 1° and exposure time of 90 s. The data were integrated and corrected by means of the CrysAlis program package, which was also used to apply empirical absorption correction using spherical harmonics, implemented in the SCALE3 ABSPACK scaling algorithm [41]. The structure was refined using the SHELXL software package [42]. The positions of H atoms could not be located. The occupancies of the octahedral and tetrahedral sites were refined using mixed site-scattering curves of Fe and Al and Si and Al, respectively. The refined occupancy of the octahedrally coordinated *M* site is $Fe_{0.72(4)}Al_{0.28(4)}$, which agrees well with the results of the chemical analyses. In order to achieve stable refinement, the occupancy of the tetrahedral *T* site was fixed at $Si_{0.564}Al_{0.436}$, in agreement with the chemical data. The final structure model was refined with anisotropic approximation for all atoms, except for O4, which could not be refined with physically realistic anisotropic displacement parameters. The possible crystal chemical reason for this is the bridging role of the O4 atoms in linking two adjacent TO_4 tetrahedra (*T* = Si, Al); we suppose that some disorder is observed with regard to the orientation of the silicate sheets in adjacent 1:1 layers, which results in different rotations of tetrahedra around the *c* axis (see discussion below). Crystal data, data collection information, and structure refinement details are given in Table 2; atom coordinates and displacement parameters are in Table 3, and selected interatomic distances are in Table 4.

Table 2. Crystal data and structure refinement for berthierine.

Crystal data	
Chemical formula	$Fe^{2+}_{1.99}Al_{1.79}Mg_{0.03}Mn_{0.04}Si_{1.15}O_9H_4$
M_r	
Crystal system, space group	Hexagonal, $P6_3cm$
Temperature (K)	296(2)
a, c (Å)	5.3903(4), 14.0146(10)
V (Å^3)	352.64(6)
Z	2
μ (mm^{-1})	4.612
ρ (g/cm^3)	3.227
Crystal size (mm^3)	0.03 × 0.03 × 0.08
Data collection parameters	
Diffractometer	Rigaku XtaLAB Synergy-S
Radiation type	Mo$K\alpha$
Absorption correction	Gaussian
$2\Theta_{min}$, $2\Theta_{max}$	2.907, 27.986
No. of measured, independent and observed [$I > 2\sigma(I)$] reflections	3355, 339, 338
R_{int}	0.037
Refinement parameters	
R_1 [$F^2 > 2\sigma(F^2)$], $wR(F^2)$, S	0.053, 0.110, 1.157
No. of reflections	338
No. of parameters	27
$\Delta\rho_{max}$, $\Delta\rho_{min}$ (e Å^{-3})	0.884, −1.470

Table 3. Atomic coordinates and displacement parameters (Å^2) for berthierine.

Atom	x	y	z	U_{eq}	U_{11}	U_{22}	U_{33}	U_{23}	U_{13}	U_{12}
M *	0.3361(6)	0	0.2570(1)	0.0107(7)	0.009(1)	0.009(1)	0.0141(9)	0	−0.001(1)	0.0046(7)
T **	2/3	1/3	0.4541(3)	0.007(1)	0.006(2)	0.006(2)	0.009(2)	0	0.000	0.0030(8)
O1	2/3	1/3	0.3331(9)	0.018(3)	0.020(5)	0.020(5)	0.012(6)	0	0.000	0.010(3)
O_h2	0	0	0.331(1)	0.019(5)	0.026(8)	0.026(8)	0.007(8)	0	0.000	0.013(4)
O_h3	0.669(3)	0	0.1883(7)	0.020(3)	0.027(5)	0.025(7)	0.007(5)	0	−0.003(5)	0.013(4)
O4 ***	0	0.444(2)	0.4936(7)	0.010(2)						

* site occupancy—$Fe_{0.72(4)}Al_{0.28(4)}$; ** site occupancy—$Si_{0.564}Al_{0.436}$; *** refined isotropically.

Table 4. Selected interatomic distances (Å) for the crystal structure of berthierine.

M—O_h3	2.036(14)	T—O4	1.679(4) 3×
M—O_h3	2.040(8) 2×	T—O1	1.696(15)
M—O1	2.083(7) 2×	<T—O>	1.683
M—O_h2	2.087(9)		
<M—O>	2.055		

3. Results

The only crystallographic information on berthierine available so far was the unit-cell parameters for two berthierine polytypes studied by Brindley in 1951 [39], who reported orthorhombic (a = 5.391, b = 9.333, c = 7.040 Å) and monoclinic (a = 5.411, b = 9.333, c = 7.040 Å, β = 104.5°) varieties. Bertoldi et al. [18] synthesized berthierine as a metastable precursor to chamosite (see below) and determined the following unit-cell parameters for the synthetic sample with the composition $(Fe^{2+}_{1.83}Al_{0.67}Fe^{3+}_{0.33})_{\Sigma 2.83}[Si_{1.33}Al_{0.67}O_5](OH)_4$: a = 5.388, b = 9.377, c = 7.040 Å, α = 89.96, β = 104.5, γ = 90.16°, indicating the triclinic

symmetry of their material. No atom coordinates have ever been published for berthierine, and our study is the first report on detailed structure determination for this interesting and important mineral.

The crystal structure of berthierine from Lovozero is shown in Figure 2a. The mineral belongs to the kaoline-serpentine group of 1:1 phyllosilicates, which means that it is based upon double layers formed by trioctahedral sheets of MO_6 octahedra and $[T_2O_5]$ aluminosilicate sheets of corner-sharing TO_4 tetrahedra (Figure 2b).

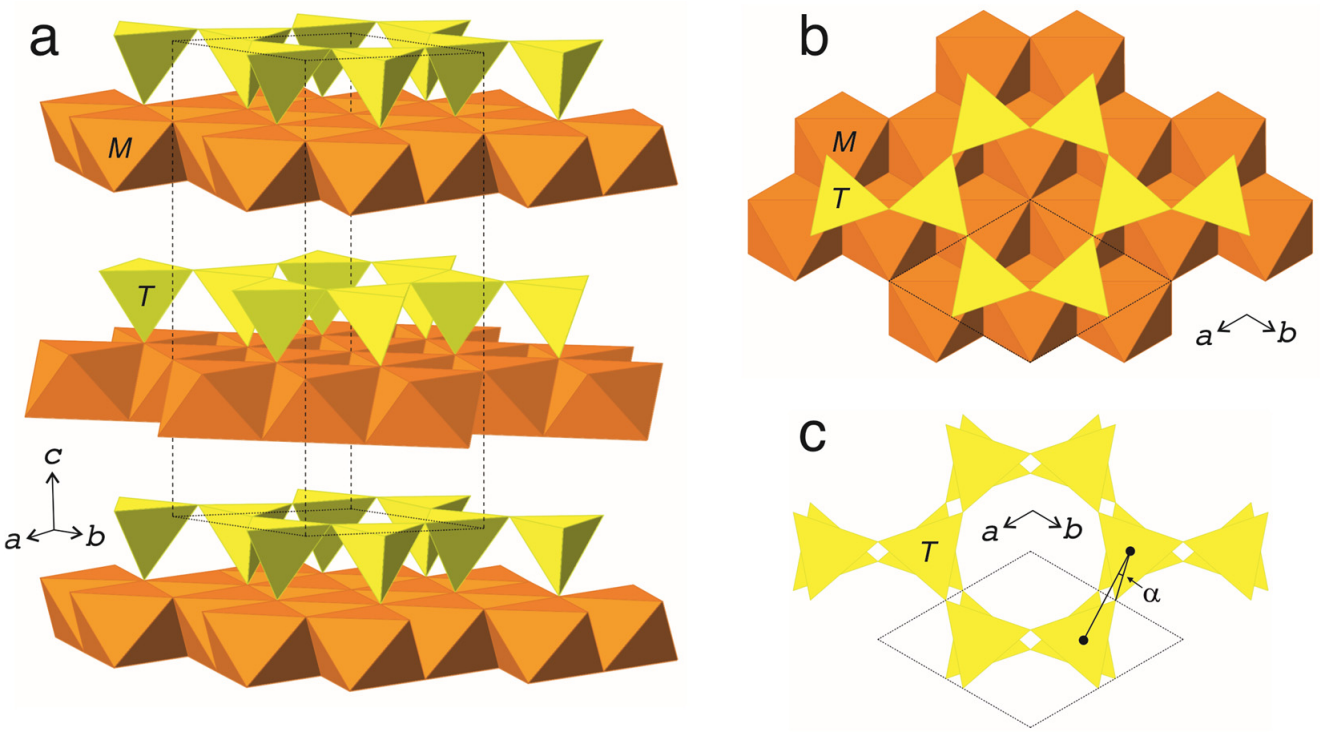

Figure 2. The crystal structure of berthierine-2H_1 from Lovozero: general overview (**a**), projection of the 1:1 layer (**b**), mutual orientation of two subsequent silicate sheets with an indication of the ditrigonal rotation angle α (**c**).

There is one crystallographically independent octahedrally coordinated *M* site with an average <*M*-O> distance of 2.055 Å. Taking into account the average $^{VI}Al^{3+}$-O and $^{VI}Fe^{2+}$-O distances of 1.904 and 2.147, respectively [43,44], and, assuming the approximate ratio Fe^{2+}:Al^{3+} = 2:1, the expected <*M*-O> distance is 2.066 Å, well in agreement with the experimental value. Similarly, for one crystallographically independent *T* site with the Si^{4+}:Al^{3+} ratio of ca. 1:1, the expected <*T*-O> distance (taking into account average $^{IV}Si^{4+}$-O and $^{IV}Al^{3+}$-O distances of 1.625 and 1.746 Å, respectively [45]) is 1.686 Å, in good agreement with the experimental value of 1.683 Å.

In phyllosilicates, the six-membered silicate rings are usually distorted according to the mechanism known as a ditrigonal rotation [46], resulting from the adaptation of silicate anion to interlayer cation or hydrogen bonding. The rotation angle, α, may assume positive or negative values depending upon the position of the bridging O atom that may move forward or backward from the octahedral cation of the same layer [47]. In berthierine, $\alpha = +20.8^\circ$, and ditrigonal distortions of silicate sheets in the adjacent layers are opposite to one another (Figure 2c).

4. Discussion

4.1. End-Member Chemical Formula

As was pointed out above, the idealized chemical formula of bethierine from Lovozero can be written as $^{VI}(Fe^{2+}{}_2Al)[^{IV}(SiAl)O_5](OH)_4$, assuming one octahedral and one tetrahedral site with total cation disorder in each site. The ideal chemical formula of berthierine approved by the International Mineralogical Association is $(Fe^{2+},Fe^{3+},Al)_3(Si,Al)_2O_5(OH)_4$, suggesting an end-member chemical formula $^{VI}Fe^{2+}{}_3[^{IV}Si_2O_5](OH)_4$. This corresponds to the berthierine sample reported here with Fe^{2+} predominant at the octahedral site and Si^{4+} predominant at the tetrahedral site. Any cation ordering with the decrease of symmetry from the ideal $P6_3cm$ space group would correspond to a separate mineral species, which opens up the possibility of future discoveries of new mineral species in the kaolinite-serpentine group that should be regulated by some nomenclature rules absent in the current literature.

4.2. Polytype Identification and Symmetry

Taking into account the large amount of work done on berthierine, it is rather remarkable how little crystallographic information is available on this mineral, which can be explained by its occurrence as fine-grained aggregates and its poor crystallinity. As has already been mentioned, Brindley [39] identified two polytypes of berthierine, orthorhombic and monoclinic, whereas Bertoldi et al. [18] reported triclinic cells for a synthetic analog of berthierine. The different symmetries reported for berthierine as well as the hexagonal symmetry reported here most probably correspond to different polytypes or species with different degrees of cation ordering; the unambiguous explanation is currently impossible, taking into account the absence of direct structure determinations, except for the one presented in this paper.

In our study, the overall hexagonal symmetry of berthierine from Lovozero was found with the space group $P6_3cm$, which is characteristic of the $2H_1$ polytypes of the 1:1 serpentine-group minerals. In fact, berthierine from Lovozero is isotypic to lizardite-$2H_1$, $Mg_3[Si_2O_5](OH)_4$, described by Mellini and Zanazzi from Coli, Italy [47]. Its unit-cell dimensions (a = 5.318, c = 14.541 Å) can be compared with those of berthierine-$2H_1$ reported herein (a = 5.3903, c = 14.0146 Å). The a parameter of berthierine is significantly larger than that of lizardite, whereas the c parameter is shorter. The explanation for such a behavior lies in the mechanism of mutual geometric adaptation between the octahedral and tetrahedral sheets, which is achieved through the ditrigonal rotation on one hand and octahedral flattening on the other. The latter is characterized by the octahedral flattening angle (ψ), which is calculated according to the following formula [46]:

$$\psi = arccos[(\text{octahedral thickness})/(2\langle M\text{-O}\rangle)], \quad (1)$$

where octahedral thickness is measured as the distance between the planes of opposite triangular faces of octahedra parallel to the plane of the octahedral sheet.

It is worth noting that the <*M*-O> distances for berthierine-$2H_1$ and lizardite-$2H_1$ are not very different, 2.087 and 2.067 Å, respectively. However, their ψ values are 61.5 and 59.8°, respectively, which means that the MO_6 octahedra in berthierine are essentially flattened compared to those in lizardite. The octahedral flattening is explained by the larger dimensions of the aluminosilicate sheets in berthierine compared to the almost pure silicate sheets in lizardite. The ditrigonal rotation parameter in lizardite-$2H_1$ is +6.4°, much smaller than that in berthierine-$2H_1$ (+20.8°).

Zheng and Bailey [48] reported on the crystal structure of the $2H_1$ polytype of amesite, $(Mg_2Al)[(SiAl)O_5](OH)_4$, which is an Mg analog of berthierine. They found distortions

of the crystal structure from an ideal configuration with the $P6_3cm$ symmetry and refined it in the non-standard triclinic $C\bar{1}$ space group with the unit-cell parameters a = 5.299, b = 9.181, c = 14.050 Å, α = 90.06, β = 90.30, γ = 90.00°, and V = 683.6 Å^3. The partial ordering was reported for both octahedral and tetrahedral sites with the <*M*-O> bond lengths in the range of 2.003–2.080 Å and the <*T*-O> bond lengths in the range of 1.671–1.710 Å. The ditrigonal rotation angle α is equal to +15.6 and 14.8° for two independent silicate sheets, approaching the value observed for berthierine-2H_1. The octahedral flattening parameters ψ vary from 59.9 to 61.0° (<ψ> = 60.4°), indicating a rather flattened average configuration of MO_6 octahedra, which explains the value of the c parameter close to that of berthierine-2H_1. In contrast to the crystal of amesite-2H_1 studied in [48], no indications of cation ordering (e.g., additional reflections or satellites violating X-ray diffraction absence conditions) had been observed for berthierine-2H_1.

4.3. Structural Complexity and Relative Stability of Berthierine and Chamosite

As has been mentioned in the introduction, the formation of berthierine, at least in some geochemical environments, proceeds in accord with the metastable crystallization scenario defined by the Ostwald rule of stages [23], where berthierine forms prior to the formation of its chemical analog (polymorph) chamosite (see also: [49]). As pointed out by Bertoldi et al. [16,18], this is the general observation for the formation of a serpentine-group mineral preceding the formation of a chlorite-group mineral, observed in both nature and experiment. The Goldsmith rule [28,38] states that metastable phases formed in Ostwald sequences are usually structurally simpler and more disordered than the stable final phases. The crystal-structure model for berthierine reported in this work allows us to verify the validity of the Goldsmith rule for the pair berthierine-chamosite using the information-based parameters of structural complexity developed in [29,50,51].

According to this approach, structural complexity can be estimated as the amounts of Shannon information per atom ($^{str}I_G$) and per unit cell ($^{str}I_{G,total}$) by means of the following equations:

$$^{str}I_G = -\sum_{i=1}^{k} p_i \log_2 p_i (\text{bit/atom}), \quad (2)$$

$$^{str}I_{G,total} = -v\sum_{i=1}^{k} p_i \log_2 p_i (\text{bit/cell}), \quad (3)$$

where information is measured in binary digits (bits), k is the number of different crystallographic orbits (Wyckoff sites) in the structure, and p_i is the random choice probability for an atom from the ith crystallographic orbit, that is:

$$p_i = m_i/v, \quad (4)$$

where m_i is a multiplicity of a crystallographic orbit (i.e., the number of atoms of a specific Wyckoff site in the reduced unit cell) and v is the total number of atoms in the reduced unit cell.

The only full report on the crystal structure of chamosite is that of its Mg-rich II*b* polytype determined by Walker and Bish [52] (Figure 3a). Similar to those of other chlorite-group minerals, the crystal structure of chamosite is based upon two types of layers: a 2:1 layer of trioctahedral sheet sandwiched between two tetrahedral [T_2O_5] sheets (Figure 3b) and a trioctahedral sheet of edge-sharing (MO_6) octahedra (Figure 3c). The layers are stacked along the c axis in an alternating fashion and are linked by hydrogen bonding only. It should be noted that the crystal structure of chamosite-II*b* reported in [52] possesses a certain degree of cation ordering absent in berthierine-2H_1 reported herein.

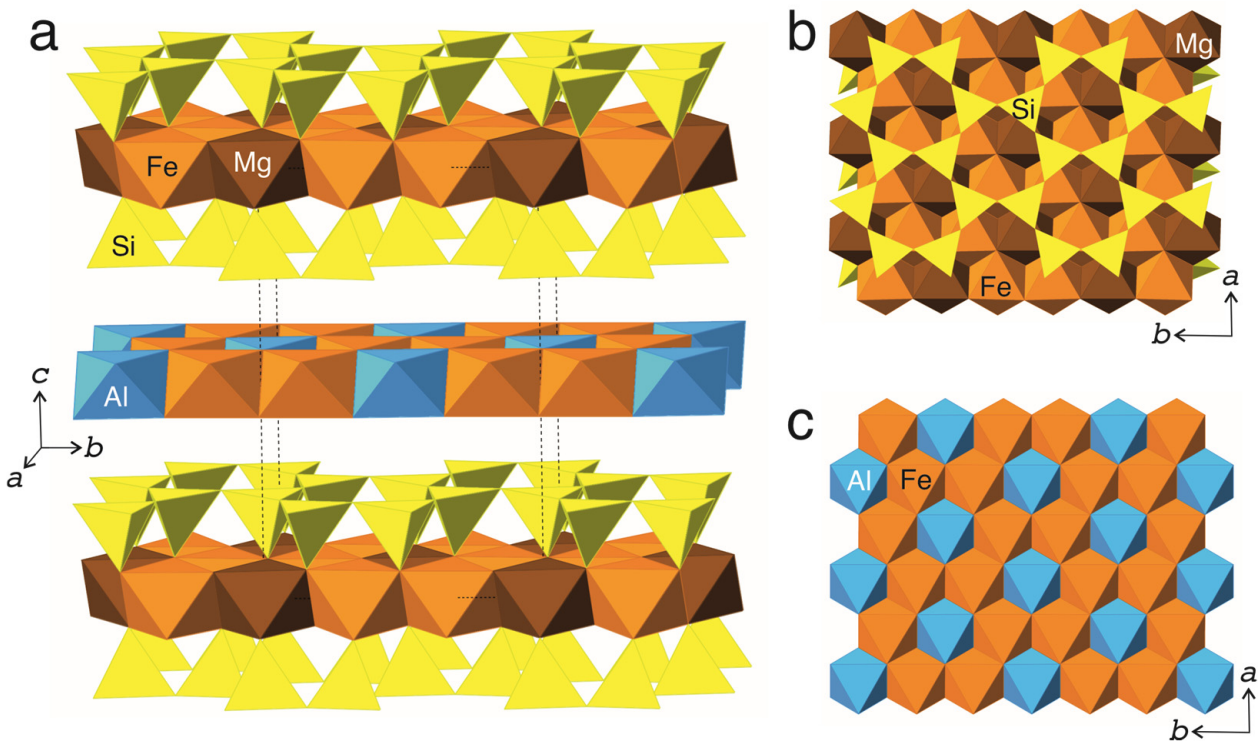

Figure 3. The crystal structure of chamosite-II*b* (**a**) and projections of the $M_3[T_2O_5]_2(OH)_2$ (**b**) and $M(OH)_2$ (**c**) layers perpendicular to [001].

The information-based structural complexity parameters for berthierine-2H_1 and chamosite-II*b* calculated according to Equations (2)–(4) are given in Table 5, which also contains thermodynamic data on both minerals available from literature (the chemical composition is given for each particular sample). In order to calculate the correct values of structural information including contributions from H atoms not determined from X-ray diffraction analysis, the procedure of H-correction was applied as described in [51,53].

Table 5. Structural complexity and thermodynamic parameters for berthierine and chamosite.

Chemical Formula	I_G [Bit/Atom]	$I_{G,total}$ [Bit/Cell]	$\Delta_f H^\circ_{298}$, kJ·mol^{-1}	S°_{298}, J·mol^{-1}K^{-1}	$\Delta_f G^\circ_{298}$, kJ·mol^{-1}	Ref.
Berthierine *						
$(Fe^{2+}_{1.99}Al_{0.94}Mg_{0.03}Mn_{0.04})$ $[(Si_{1.15}Al_{0.85})_{\Sigma 2.00}O_5](OH)_{3.92}O_{0.08}$	2.891	104.078				This work
$2\{(Fe^{2+}_{1.422}Al_{0.975}Fe^{3+}_{0.182}Mg_{0.157}Li_{0.035}Mn_{0.002})$ $[(Si_{1.332}Al_{0.668})O_5](OH)_4\}$			−6944.56	514.54	−7548.92	[20]
$2\{(Fe^{2+}_{1.44}Al_{0.976}Fe^{3+}_{0.182}Mg_{0.157})$ $[(Si_{1.332}Al_{0.668})O_5](OH)_4\}$			−6936.62	514.00	−7548.92	[20]
$2\{(Fe_{2.5}Al_{0.5})[Si_{1.5}Al_{0.5}O_5](OH)_4\}$				568.2	−7140.60	[18]
Chamosite						
$(Fe^{2+}_{2.72}Al_{1.33}Mn_{0.08}\square_{0.10})$ $[(Si_{2.85}Al_{1.145}Ti_{0.005})O_{10}](OH)_8$	4.225	152.117				[52]
$(Fe^{2+}_5Al)[(Si_3Al)O_{10}](OH)_8$			−7120.85	559.4		[17]
$(Fe^{2+}_4Al_2)[(Si_2Al_2)O_{10}](OH)_8$			−7607.46	514.8		[19]

* Thermodynamic parameters for berthierine are given for two formula units in order to ease the comparison with the parameters for chamosite.

The relative stability of berthierine and chamosite was a subject of extensive discussion in the literature [20,54–57]. The problem is complicated by the variability of chemical compositions of both berthierine and chamosite. Blanc et al. [20] considered the following reaction of transition from berthierine to chamosite of the same composition:

$$2[(Fe^{2+}_{1.422}Al_{0.975}Fe^{3+}_{0.182}Mg_{0.157}Li_{0.035}Mn_{0.002})(Si_{1.332}Al_{0.668})O_5(OH)_4 \text{ (berthierine)}] \rightarrow (Fe^{2+}_{2.844}Al_{1.95}Fe^{3+}_{0.364}Mg_{0.314}Li_{0.07}Mn_{0.004})(Si_{2.664}Al_{1.336})O_{10}(OH)_8 \text{ (chamosite)}$$

The corresponding Gibbs energy of this reaction was estimated to be in the range from 86 to 88 kJ mol^{-1} at 25 and 150 °C, respectively, indicating that, for the same composition, berthierine is significantly less stable than chamosite [20]. However, berthierine may crystallize and persist metastably in natural environments, especially low-temperature ones, as outlined in the introduction. In general, the comparison of thermodynamic parameters for both minerals shows that chamosite is more stable than berthierine, whereas the structural complexity calculations indicate that it is also more complex, which conforms to the Goldsmith rule: in an Ostwald sequence of polymorph crystallization, metastable phases are simpler and more disordered than their stable counterparts. As was put out by Goldsmith [28], structurally simpler phases crystallize more easily, which may be related to the smaller size of their critical nuclei [58], their lower densities, and their lower interfacial energies [38] compared to the stable and more complex phases.

4.4. Note on Relative Topological Complexity of Berthierine and Chamosite

The structural complexity parameters given in Table 5 are based on the experimental structure models determined from single-crystal X-ray diffraction analysis. It makes sense to consider the complexity of the serpentine- and chlorite-group minerals in topological terms, i.e., in terms of the complexity of their structural units with ideal (maximal) symmetries. Since both serpentine- and chlorite-group minerals have layered crystal structures, one should consider the topological complexities of layers that serve as bases for the respective structure types. Figure 4 shows the ideal versions of basic layers in the crystal structures of serpentine- and chlorite-group minerals: the $[M(OH)_2]$ layer of edge-sharing $M(OH)_6$ octahedra from chlorite-group minerals (Figures 3c and 4a), the 1:1 heteropolyhedral $[M_3[T_2O_5](OH)_4]$ layer in serpentine-group minerals (Figures 2b and 4b), and the 2:1 heteropolyhedral layer $M_3[T_2O_5]_2(OH)_2$ in chlorite-group minerals (Figures 3b and 4c). The ideal layer groups of the layers are given in Figure 4d,e,f, respectively, whereas Table 6 provides ideal symmetries, independent site distributions, and topological complexity parameters of the layers. The minimal total topological complexity of the double-layer structure of chlorite-group minerals can be calculated, taking into account the equation $M_6[T_2O_5]_2(OH)_8 = M_3[T_2O_5]_2(OH)_2 + 3M(OH)_2$, as 60.239 + 3 × 7.610 = 83.069 bit/cell. On the other hand, the serpentine-type 1:1 layers possess 52.039 bit/cell only. Therefore, from the viewpoint of topological information, serpentine-group minerals are simpler than chlorite-group minerals, which provides additional support for the validity of the Goldsmith principle for metastable crystallization of serpentines in the stability field of chlorites.

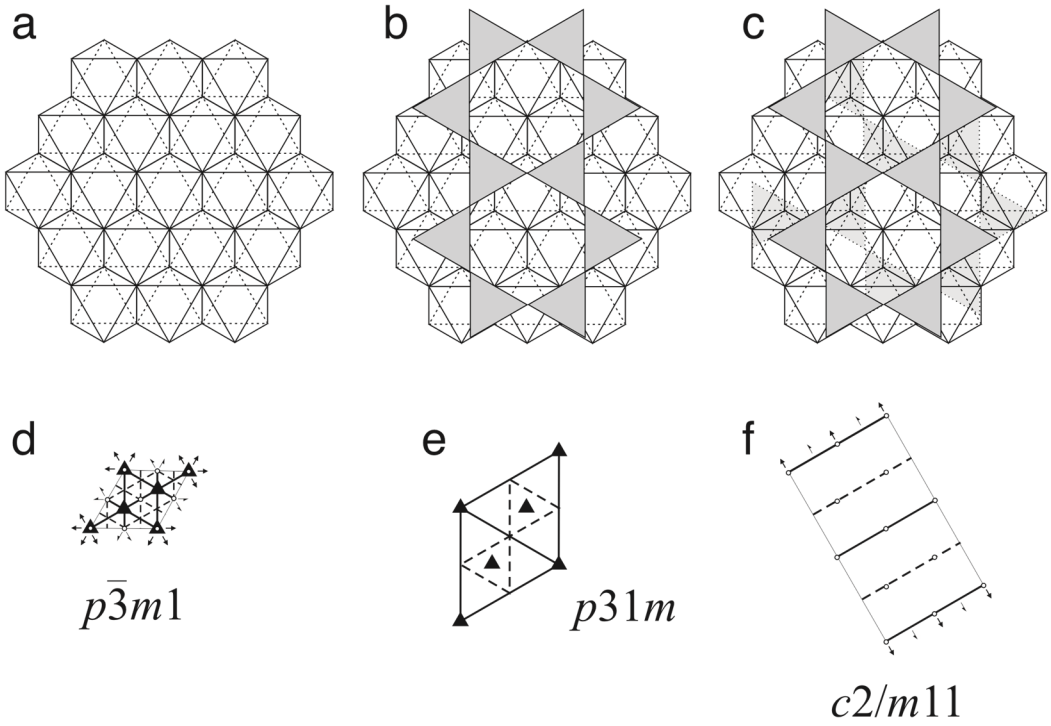

Figure 4. Idealized versions of the polyhedral layers in serpentine- and chlorite-group minerals: the $[M(OH)_2]$ layer of edge-sharing $M(OH)_6$ octahedra (**a**), the 1:1 heteropolyhedral $[M_3[T_2O_5](OH)_4]$ layer (**b**), and the 2:1 heteropolyhedral layer $M_3[T_2O_5]_2(OH)_2$ (**c**). Layer symmetry groups are given for the three layers in (**d**,**e**,**f**), respectively.

Table 6. Ideal symmetries, independent site distributions, and topological complexity parameters of layers in the crystal structures of serpentine- and chlorite-group minerals.

Mineral Group	**Serpentine**	**Chlorite**	
General formula	$M_3[T_2O_5](OH)_4$	$M_6[T_2O_5]_2(OH)_8 = M_3[T_2O_5]_2(OH)_2 + 3M(OH)_2$	
Layer formula	$M_3[T_2O_5](OH)_4$	$M(OH)_2$	$M_3[T_2O_5]_2(OH)_2$
Layer symmetry group	$p31m$	$p\bar{3}m1$	$c2/m11$
Site distribution	M:[3], T:[2], O:[2+3], O_h:[3+1], H:[3+1]	M:[1], O_h:[2], H:[2]	M:[1+2], T:[4], O:[2+4+4], O_h:[2], H:[2]
I_G [bit/atom]	2.891	1.522	2.869
$I_{G,total}$ [bit/cell]	52.039	7.610	60.239

5. Conclusions

The results of the present study of berthierine from hydrothermal veins of the Lovozero alkaline massif, Kola peninsula, Russian Arctic, provide the first crystal-structure determination for this mineral and demonstrate that the Lovozero sample belongs to the $2H_1$ polytype with overall hexagonal symmetry and the highest possible for this polytype space group $P6_3cm$. In natural environments and experiments, berthierine (a serpentine-group mineral) usually forms metastable prior to the formation of its polymorph chamosite, a chlorite-group mineral. Thus, the berthierine crystallization is in agreement with the Ostwald rule of stages that postulates the step-like phase formation with increasing thermodynamic stability [23]. According to Goldsmith [28], in Ostwald cascades, metastable phases are usually structurally simpler and more disordered than stable phases, which agrees with the calculations of structural and topological complexity parameters for berthierine and chamosite. Moreover, this observation is also valid and can be applied to the general case of

metastable serpentine-group minerals' crystallization and their subsequent transformation into chlorite-group minerals.

Author Contributions: Conceptualization, S.V.K. and V.N.Y.; methodology, S.V.K., O.F.G., Y.A.P.; validation, S.V.K. and V.G.K.; formal analysis, S.V.K., O.F.G. and Y.A.P.; investigation, S.V.K., V.N.Y., O.F.G. and Y.A.P.; data curation, S.V.K.; writing—original draft preparation, S.V.K.; writing—review and editing, V.N.Y. and V.G.K.; visualization, S.V.K. and Y.A.P.; supervision, S.V.K.; project administration, S.V.K.; funding acquisition, S.V.K. All authors have read and agreed to the published version of the manuscript.

Funding: This research in X-ray diffraction, crystal chemistry, and stability-complexity fields was funded by the Russian Science Foundation, grant number 24-17-00083, https://rscf.ru/project/24-17-00083/ (accessed on 24 December 2024). The part in mineralogical description and chemical analysis was funded by the state task FMEZ-2024-0008 of the Geological Institute of KSC RAS.

Data Availability Statement: The crystal structure data for berthierine are available as CIF–file from the CCDC/FIZ Karlsruhe database as CSD # 2408096 at https://www.ccdc.cam.ac.uk (accessed on 24 December 2024).

Acknowledgments: The X-ray diffraction and chemical analytical studies were performed in the FRC KSC RAS Centre for Collective Use of Equipment.

Conflicts of Interest: The authors declare no conflicts of interest.

References

1. Toth, T.A.; Fritz, S.J. An Fe-Berthierine From A Cretaceous Laterite: Part I. Characterization. *Clays Clay Miner.* **1997**, *45*, 564–579. [CrossRef]
2. Fritz, S.J.; Toth, T.A. An Fe-Berthierine from a Cretaceous Laterite: Part II. Estimation of Eh, pH and pCO_2 Conditions of Formation. *Clays Clay Miner.* **1997**, *45*, 580–586. [CrossRef]
3. Kodama, H.; Foscolos, A.E. Occurrence of Berthierine in Canadian Arctic Desert Soils. *Can. Mineral.* **1981**, *19*, 279–283.
4. Iljima, A.; Matsumoto, R. Berthierine and Chamosite in Coal Measures of Japan. *Clays Clay Miner.* **1982**, *30*, 264–274. [CrossRef]
5. Nikulin, I.I.; Starostin, V.I.; Samsonov, A.A. Pre-Visean Bauxites and Iron-Aluminum Ores Deposit of the KMA and Prospects for Development. *Geol. Ore Depos.* **2021**, *63*, 368–381. [CrossRef]
6. Savko, A.D.; Ovchinnikova, M.Y.; Boeva, N.M. Berthierine-Rich Bauxites in the Kursk Magnetic Anomaly (KMA). *Lithol. Miner. Resour.* **2021**, *56*, 49–55. [CrossRef]
7. Steiner, T.M.C.; Gawlick, H.-J.; Melcher, F.; Schlagintweit, F. Ophiolite Derived Material as Parent Rocks for Late Jurassic Bauxite: Evidence for Tithonian Unroofing in the Northern Calcareous Alps (Eastern Alps, Austria). *Int. J. Earth Sci.* **2021**, *110*, 1847–1862. [CrossRef]
8. Savko, A.D.; Nikulin, I.I.; Ovchinnikova, M.Y.; Boeva, N.M. Historical-Genetic Analysis of the Formation of High-Grade Iron Ores and Related Bauxites in the Kursk Magnetic Anomaly (Russia). *Lithol. Miner. Res.* **2022**, *57*, 290–298. [CrossRef]
9. Ali Khoudja, S.A.; Chellat, S.; Hacini, M.; Semiani, A. Petrography and Authigenic Chlorite in the Siegenian Reservoir Rocks, Berkine Basin, Eastern Algerian Sahara. *Arab. J. Geosci.* **2020**, *13*, 767. [CrossRef]
10. Poluektov, V.V.; Petrov, V.A.; Andreeva, O.V. Migration and Sorption of Uranium in Various Redox Conditions on the Example of Volcanic-Related Deposits in the Streltsovka Caldera, SE Transbaikalia. *Geol. Ore Dep.* **2021**, *63*, S29–S61. [CrossRef]
11. Petrov, V.A.; Andreeva, O.V.; Poluektov, V.V. The Character of Magmatism, Hydrothermal-Metasomatic, and Filtration-Transport Processes in Uranium-Bearing Volcanic-Related Structures. *J. Volcanol. Seismol.* **2023**, *17*, 353–373. [CrossRef]
12. Pribavkin, S.V.; Soroka, E.I.; Azovskova, O.B.; Smoleva, I.V.; Leonova, L.V.; Gottman, I.A.; Sustavov, S.G.; Rovnushkin, M.Y. Association of Siderite with Iron Sulfides and Silicates in Rocks of the Mikheevskoe Cu(Mo,Au) Porphyry Deposit (Southern Urals). *Geol. Ore Dep.* **2023**, *65*, 332–345. [CrossRef]
13. Xi, J.; Yang, Y.; He, H.; Xian, H.; Tan, W.; Li, R.; Zhu, J.; Xu, H. Microstructural and Compositional Evolutions during Transformation from Biotite to Berthierine: Implications for Phyllosilicate Alteration Processes. *Am. Mineral.* **2024**, *109*, 656–666. [CrossRef]
14. Wise, M.A. Crystallization of 'pocket' berthierine from the Pulsifer granitic pegmatite, Poland, Maine, USA. *Clays Clay Miner.* **2007**, *55*, 583–592. [CrossRef]
15. Pekov, I.V.; Chukanov, N.V.; Turchkova, A.G.; Grishin, V.G. News in mineralogy of the Lovozero massif. *Tr. Fersmanovskoy Sess. GI KCS RAS* **2004**, 30–33. (In Russian)

16. Bertoldi, C.; Benisek, A.; Cemic, L.; Dachs, E. The Heat Capacity of Two Natural Chlorite Group Minerals Derived from Differential Scanning Calorimetry. *Phys. Chem. Miner.* **2001**, *28*, 332–336. [CrossRef]
17. Vidal, O.; Parra, T.; Trotet, F. A Thermodynamic Model for Fe-Mg Aluminous Chlorite Using Data from Phase Equilibrium Experiments and Natural Pelitic Assemblages in the 100° to 600 °C, 1 to 25 Kb Range. *Am. J. Sci.* **2001**, *301*, 557–592. [CrossRef]
18. Bertoldi, C.; Dachs, E.; Cemic, L.; Theye, T.; Wirth, R.; Groger, W. The heat capacity of the serpentine subgroup mineral berthierine $(Fe_{2.5}Al_{0.5})[Si_{1.5}Al_{0.5}O_5](OH)_4$. *Clays Clay Miner.* **2005**, *53*, 380–388. [CrossRef]
19. Vidal, O.; Parra, T.; Vieillard, P. Thermodynamic Properties of the Tschermak Solid Solution in Fe-Chlorite: Application to Natural Examples and Possible Role of Oxidation. *Am. Mineral.* **2005**, *90*, 347–358. [CrossRef]
20. Blanc, P.; Gailhanou, H.; Rogez, J.; Mikaelian, G.; Kawaji, H.; Warmont, F.; Gaboreau, S.; Grangeon, S.; Grenèche, J.-M.; Vieillard, P.; et al. Thermodynamic Properties of Chlorite and Berthierine Derived from Calorimetric Measurements. *Phys. Chem. Miner.* **2014**, *41*, 603–615. [CrossRef]
21. James, R.S.; Turnock, A.C.; Fawcett, J.J. The Stability and Phase Relations of Iron Chlorite below 8.5 Kb P_{H2O}. *Contrib. Mineral. Petrol.* **1976**, *56*, 1–25. [CrossRef]
22. Cho, M.; Fawcett, J.J. A Kinetic Study of Clinochlore and Its High Temperature Equivalent Forsterite-Cordierite-Spinel at 2 Kbar Water Pressure. *Am. Mineral.* **1986**, *71*, 68–77.
23. Ostwald, W. Studien Über Die Bildung Und Umwandlung Fester Körper. 1. Abhandlung: Übersättigung Und Überkaltung. *Z. Physik. Chem.* **1897**, *22*, 289–330. [CrossRef]
24. Nývlt, J. The Ostwald Rule of Stages. *Cryst. Res. Technol.* **1995**, *30*, 443–449. [CrossRef]
25. Threlfall, T. Structural and Thermodynamic Explanations of Ostwald's Rule. *Org. Process Res. Dev.* **2003**, *7*, 1017–1027. [CrossRef]
26. Hedges, L.O.; Whitelam, S. Limit of Validity of Ostwald's Rule of Stages in a Statistical Mechanical Model of Crystallization. *J. Chem. Phys.* **2011**, *135*, 164902. [CrossRef]
27. Cardew, P.T. Ostwald Rule of Stages–Myth or Reality? *Cryst. Growth Des.* **2023**, *23*, 3958–3969. [CrossRef]
28. Goldsmith, J.R. A "simplexity principle" and its relation to "ease" of crystallization. *J. Geol.* **1953**, *61*, 439–451. [CrossRef]
29. Krivovichev, S.V. Structural complexity of minerals: Information storage and processing in the mineral world. *Mineral. Mag.* **2013**, *77*, 275–326. [CrossRef]
30. Cempírek, J.; Grew, E.S.; Kampf, A.R.; Ma, C.; Novák, M.; Gadas, P.; Škoda, R.; Vašinová-Galiová, M.; Pezzotta, F.; Groat, L.A.; et al. Vránaite, ideally $Al_{16}B_4Si_4O_{38}$, a new mineral related to boralsilite, $Al_{16}B_6Si_2O_{37}$, from the Manjaka pegmatite, Sahatany Valley, Madagascar. *Amer. Mineral.* **2016**, *101*, 2108–2117. [CrossRef]
31. Zaitsev, A.N.; Zhitova, E.S.; Spratt, J.; Zolotarev, A.A.; Krivovichev, S.V. Isolueshite, $NaNbO_3$, from the Kovdor carbonatite, Kola peninsula, Russia: Composition, crystal structure and possible formation scenarios. *N. Jb. Mineral. Abh.* **2017**, *194*, 165–173. [CrossRef]
32. Krivovichev, S.V. Hydrogen bonding and structural complexity of the $Cu_3(AsO_4)(OH)_3$ polymorphs (clinoclase, gilmarite): A theoretical study. *J. Geosci.* **2017**, *62*, 79–85. [CrossRef]
33. Krivovichev, S.V.; Hawthorne, F.C.; Williams, P.A. Structural complexity and crystallization: The Ostwald sequence of phases in the $Cu_2(OH)_3Cl$ system (botallackite–atacamite–clinoatacamite). *Struct. Chem.* **2017**, *28*, 153–159. [CrossRef]
34. Plášil, J. Structural complexity of uranophane and uranophane-β: Implications for their formation and occurrence. *Eur. J. Mineral.* **2018**, *30*, 253–257. [CrossRef]
35. Huskić, I.; Novendra, N.; Lim, D.-W.; Topić, F.; Titi, H.M.; Pekov, I.V.; Krivovichev, S.V.; Navrotsky, A.; Kitagawa, H.; Friščić, T. Functionality in metal-organic framework minerals: Proton conductivity, stability and potential for polymorphism. *Chem. Sci.* **2019**, *10*, 4923–4929. [CrossRef] [PubMed]
36. Zolotarev, A.A.; Krivovichev, S.V.; Panikorovskii, T.L.; Gurzhiy, V.V.; Bocharov, V.N.; Rassomakhin, M.A. Dmisteinbergite, $CaAl_2Si_2O_8$, a Metastable Polymorph of Anorthite: Crystal-Structure and Raman Spectroscopic Study of the Holotype Specimen. *Minerals* **2019**, *9*, 570. [CrossRef]
37. Kolitsch, U.; Weil, M.; Kovrugin, V.M.; Krivovichev, S.V. Crystal Chemistry of the Variscite and Metavariscite Groups: Crystal Structures of Synthetic $CrAsO_4{\cdot}2H_2O$, $TlPO_4{\cdot}2H_2O$, $MnSeO_4{\cdot}2H_2O$, $CdSeO_4{\cdot}2H_2O$ and Natural Bonacinaite, $ScAsO_4{\cdot}2H_2O$. *Miner. Mag.* **2020**, *84*, 568–583. [CrossRef]
38. Krivovichev, S.V. Metastable Crystallization and Structural Complexity of Minerals. *Dokl. Earth Sci.* **2022**, *507*, 1040–1043. [CrossRef]
39. Brindley, G.W. The Crystal Structure of Some Chamosite Minerals. *Miner. Mag.* **1951**, *29*, 502–525.
40. Brindley, G.W. Chemical Compositions of Berthierines—A Review. *Clays Clay Miner.* **1982**, *30*, 153–155. [CrossRef]
41. Agilent Technologies. *CrysAlisPro*, Version 1.171.36.20; Agilent Technologies: Santa Clara, CA, USA, 2012. Available online: https://www.rsc.org/suppdata/cc/c3/c3cc43513j/c3cc43513j.txt (accessed on 24 December 2024).
42. Sheldrick, G.M. A short history of SHELX. *Acta Crystallogr.* **2008**, *A64*, 112–116. [CrossRef] [PubMed]
43. Gagné, O.C.; Hawthorne, F.C. Mean Bond-Length Variations in Crystals for Ions Bonded to Oxygen. *Acta Crystallogr. B* **2017**, *73*, 1019–1031. [CrossRef]

44. Gagné, O.C.; Hawthorne, F.C. Bond-Length Distributions for Ions Bonded to Oxygen: Results for the Transition Metals and Quantification of the Factors Underlying Bond-Length Variation in Inorganic Solids. *IUCrJ* **2020**, *7*, 581–629. [CrossRef]
45. Gagné, O.C.; Hawthorne, F.C. Bond-Length Distributions for Ions Bonded to Oxygen: Metalloids and Post-Transition Metals. *Acta Crystallogr. B* **2018**, *74*, 63–78. [CrossRef]
46. Brigatti, M.F.; Malferrari, D.; Laurora, A.; Elmi, C. Structure and mineralogy of layered silicates: Recent perspectives and new trends. *EMU Notes Mineral.* **2011**, *11*, 1–71.
47. Mellini, M.; Zanazzi, P.F. Crystal Structures of Lizardite-1T and Lizardite-2H1 from Coli, Italy. *Am. Mineral.* **1987**, *72*, 943–948.
48. Zheng, H.; Bailey, S.W. Refinement of an Amesite-2H_1 Polytype from Postmasburg, South Africa. *Clays Clay Miner.* **1997**, *45*, 301–310. [CrossRef]
49. del Mar Abad-Ortega, M.; Mieto, F. Genetic and Chemical Relationships between Berthierine, Chlorite and Cordierite in Nodules Associated to Granitic Pegmatites of Sierra Albarrana (Iberian Massif, Spain). *Contrib. Mineral. Petrol.* **1995**, *120*, 327–336. [CrossRef]
50. Krivovichev, S.V. Topological Complexity of Crystal Structures: Quantitative Approach. *Acta Crystallogr. A* **2012**, *68*, 393–398. [CrossRef]
51. Krivovichev, S.V.; Krivovichev, V.G.; Hazen, R.M.; Aksenov, S.M.; Avdontceva, M.S.; Banaru, A.M.; Gorelova, L.A.; Ismagilova, R.M.; Kornyakov, I.V.; Kuporev, I.V.; et al. Structural and chemical complexity of minerals: An update. *Mineral. Mag.* **2022**, *86*, 183–204. [CrossRef]
52. Walker, J.R.; Bish, D.L. Application of Rietveld Refinement Techniques to a Disordered II*b* Mg-Chamosite. *Clays Clay Miner.* **1992**, *40*, 319–322. [CrossRef]
53. Pankova, Y.A.; Gorelova, L.A.; Krivovichev, S.V.; Pekov, I.V. The Crystal Structure of Ginorite, $Ca_2[B_{14}O_{20}(OH)_6]\cdot 5H_2O$, and the Analysis of Dimensional Reduction and Structural Complexity in the CaO-B_2O_3-H_2O System. *Eur. J. Miner.* **2018**, *30*, 277–287. [CrossRef]
54. Wilson, J.; Savage, D.; Cuadros, J.; Shibata, M.; Ragnarsdottir, K.V. The Effect of Iron on Montmorillonite Stability. (I) Background and Thermodynamic Considerations. *Geochim. Cosmochim. Acta* **2006**, *70*, 306–322. [CrossRef]
55. Wilson, J.; Cressey, G.; Cressey, B.; Cuadros, J.; Ragnarsdottir, K.V.; Savage, D.; Shibata, M. The Effect of Iron on Montmorillonite Stability. (II) Experimental Investigation. *Geochim. Cosmochim. Acta* **2006**, *70*, 323–336. [CrossRef]
56. Bertoldi, C.; Dachs, E.; Appel, P. Heat-Pulse Calorimetry Measurements on Natural Chlorite-Group Minerals. *Am. Mineral.* **2007**, *92*, 553–559. [CrossRef]
57. Mosser-Ruck, R.; Cathelineau, M.; Guillaume, D.; Charpentier, D.; Rousset, D.; Barres, O.; Michau, N. Effects of Temperature, pH, and Iron/Clay and Liquid/Clay Ratios on Experimental Conversion of Dioctahedral Smectite to Berthierine, Chlorite, Vermiculite, or Saponite. *Clays Clay Miner.* **2010**, *58*, 280–291. [CrossRef]
58. Morse, J.W.; Casey, W.H. Ostwald Processes and Mineral Paragenesis in Sediments. *Amer. J. Sci.* **1988**, *288*, 537–560. [CrossRef]